Helicenes

Zitierweise: *Angew. Chem. Int. Ed.* **2023,** *62,* e202215468
Internationale Ausgabe: doi.org/10.1002/anie.202215468
Deutsche Ausgabe: doi.org/10.1002/ange.202215468

$(BO)_2$-Doped Tetrathia[7]helicene: A Configurationally Stable Blue Emitter

Luigi Menduti, Clara Baldoli, Simone Manetto, Michael Bolte, Hans-Wolfram Lerner, Giovanna Longhi, Claudio Villani, Emanuela Licandro, and Matthias Wagner**

Abstract: Helicenes combine two central themes in chemistry: extended π-conjugation and chirality. Heteroatom doping preserves both characteristics and allows modulation of the electronic structure of a helicene. Herein, we report the $(BO)_2$-doped tetrathia[7]helicene **1**, which was prepared from 2-methoxy-3,3′-bithiophene in four steps. **1** is formally derived by substituting two (Mes)B–O moieties in place of (H)C=C(H) fragments in two benzene rings of the parent tetrathia[7]helicene. X-ray crystallography revealed a dihedral angle of 50.26(9)° between the two terminal thiophene rings. The (*P*)-/(*M*)-**1** enantiomers were separated by chiral HPLC and are configurationally stable at room temperature. The experimentally determined enantiomerization barrier of 27.4 ± 0.1 kcal mol^{-1} is lower than that of tetrathia[7]helicene (39.4 ± 0.1 kcal mol^{-1}). The circular dichroism spectra of (*P*)- and (*M*)-**1** show a perfect mirror-image relationship. **1** is a blue emitter ($\lambda_{em} =$ 411 nm) with a photoluminescence quantum efficiency of $\Phi_{PL} = 6\,\%$ (*cf.* tetrathia[7]helicene: $\lambda_{em} \approx 405$ nm, $\Phi_{PL} =$ 5 %).

Introduction

Polycyclic aromatic hydrocarbons (PAHs) and chiral molecules are of central importance to chemistry. Helicenes, which are built from *ortho*-fused aromatic rings and have a non-planar, screw-shaped framework, combine the key attributes of both compound classes. Configurationally stable helicenes can show unique solid-state packing (due to chiral recognition), unusual molecular dynamics (as "molecular springs"), and remarkable optoelectronic properties (due to their chiral electronically excited states). The interest in helically chiral PAHs is thus particularly pronounced in the field of materials science (*e.g.*, to develop antiglare displays consisting of OLEDs in which the electroluminescence is directly circularly polarized ("CP-OLEDs")).[1] Recently, helicene chemistry has received new impetus from the replacement of selected C atoms by other p-block atoms—so-called heteroatom doping. This design tool has already proven its value for modulating the electronic structures of planar PAHs to fine-tune HOMO–LUMO gaps and various optoelectronic properties.[2] The most commonly used doping elements to date are Si, N/P, and O/S, but B atoms are rapidly catching up.

One has to distinguish between helicenes containing tri- or tetracoordinated B centers. In the first case, the sp^2-hybridized B atom has a vacant p_z orbital for conjugation with the adjacent π-electron cloud (π-p_z delocalization); in the second case, the sp^3-hybridized B atom provides energetically low-lying σ* orbitals capable of accepting π-electron density from the surrounding aryl rings (π-σ* delocalization).

Purely B(sp^2)-doped helicenes are rare.[3] In most cases, the B atom is directly bonded to a N or O atom, which leads to electronic stabilization through partial π-electron donation and is equivalent to the isoelectronic replacement of a C=C double bond by a B=N or B=O bond. Examples of corresponding BN- or BO-helicenes are **A**[4,5] or **B** (Figure 1).[6,7] For **A**, unprecedented charge-carrier inversion was observed, as its racemate and single enantiomer are good p- and n-type semiconductors, respectively. Most B(sp^3)-doped helically chiral compounds also contain B–N

[*] L. Menduti, Dr. M. Bolte, Dr. H.-W. Lerner, Prof. Dr. M. Wagner
Institut für Anorganische Chemie, Goethe-Universität Frankfurt
Max-von-Laue-Strasse 7,60438 Frankfurt (Main) (Germany)
E-mail: matthias.wagner@chemie.uni-frankfurt.de

L. Menduti, Prof. E. Licandro
Dipartimento di Chimica, Università degli Studi di Milano
Via Camillo Golgi 19, 20133 Milano (Italy)
E-mail: emanuela.licandro@unimi.it

Dr. C. Baldoli
CNR Istituto di Scienze e Tecnologie Chimiche Giulio Natta
Via Camillo Golgi 19, 20133 Milano (Italy)

S. Manetto, Prof. C. Villani
Dipartimento di Chimica e Tecnologie del Farmaco, Sapienza Università di Roma
P.le A. Moro 5, 00185 Roma (Italy)

Prof. G. Longhi
Dipartimento di Medicina Molecolare e Traslazionale, Università di Brescia
Viale Europa 11, 25123 Brescia (Italy)

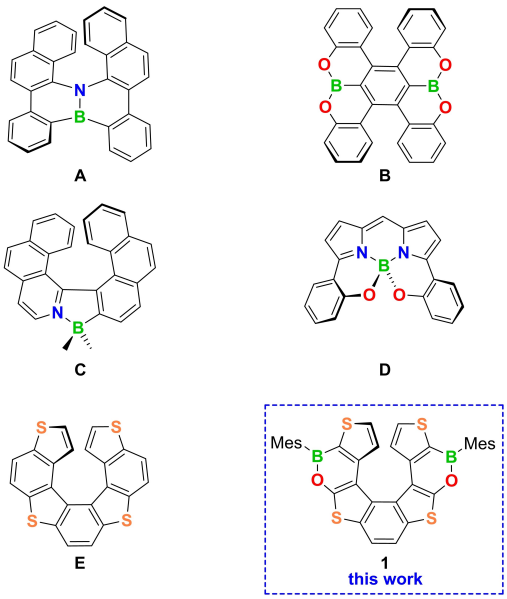

Figure 1. Examples of B(sp^2)–Het-doped helicenes **A** and **B** and of B(sp^3)–Het-doped helicenes **C** and **D** (Het = N, O). Tetrathia[7]helicene **E** and its doubly B(sp^2)–O-doped congener **1**.

pairs, but here they are joined by σ-adduct bonds, as in the helical azaborole **C**[8,9] or in BODIPY-type compounds like **D** (Figure 1).[10,11] The latter is a red emitter, which gives both a large luminescence dissymmetry factor and a high quantum yield.

Herein, we report double B(sp^2)–O doping of tetrathia-[7]helicene **E**[12,13] to generate **1** (Figure 1). **E** was chosen as the "host scaffold" for BO incorporation, because the considerable application potential of thiophene-containing organic compounds is recognized in various fields, such as non-linear optical (NLO) materials,[14] electroactive materials,[15] light-emitting devices (OLEDs),[16] and thin-film transistors (TFTs).[17,18] Moreover, the facile functionalization of the α positions of the thiophene ring is a valuable asset during synthesis, *e.g.*, when it comes to late-stage bromination reactions of BO-doped synthesis intermediates (see Scheme 1). The chiral resolution of *rac*-**1** was achieved, and the enantiomerization barrier as well as important chiroptical properties of the individual enantiomers were determined in a combined experimental and theoretical effort.

Results and Discussion

The $(BO)_2$-doped tetrathia[7]helicene **1** is accessible in 16 % overall yield via a four-step protocol by using the known starting material 2-methoxy-3,3'-bithiophene (**S1**;[19] Scheme 1). The first B-containing building block, **2**, was prepared from **S1** through demethylative O-directed electrophilic C–H borylation with BCl_3/[nBu$_4$N]I/Et$_3$N[20] and subsequent mesitylation with MesMgBr (77 %). Of high diagnostic value are the NMR signals of the CH groups in the α positions to the two S atoms of **2**: due to π-conjugation with the electron-withdrawing B- or the electron-donating O atom, the CH nuclei in the electron-poor borylated thiophene are significantly deshielded ($\delta(^1H) = 7.98$, $\delta(^{13}C) = 138.2$) compared to those in the electron-rich oxygenated thiophene ($\delta(^1H) = 6.96$, $\delta(^{13}C) = 114.8$).

Treatment of **2** with *N*-bromosuccinimide (NBS) led to the formation of **3** in 85 % yield. The Br substituent was selectively introduced next to the S atom into the oxygenated thiophene ring, as evidenced by the disappearance of the proton resonance at 6.96 ppm and by a further upfield shift of the corresponding ^{13}C resonance (from 114.8 to 103.1 ppm) as a result of the magnetic anisotropy effect of the attached Br substituent. The molecular structure of **3** was further confirmed by X-ray diffraction (Figure S43). A twofold Stille-type coupling reaction between 2 equiv of **3** and *trans*-R$_3$Sn(H)C=C(H)SnR$_3$ (R = *n*Bu) afforded *trans*-**4** in 58 % yield after column chromatography and treatment with *n*-hexane to remove small amounts of residual *cis*-**4** and *n*Bu$_3$SnBr byproduct. The 1,2-ethenediyl bridge gives rise to new resonances at $\delta(^1H) = 7.02$ and $\delta(^{13}C) = 121.6$; the configuration of *trans*-**4** was verified by X-ray crystallography (Figure S44). We also tested two alternative access routes to **4** (see Scheme S1) via Grubbs metathesis on vinylated **2** (unprecedented for BO-doped aromatics) or late-stage borylation of two 1,2-ethenediyl-linked 2-methoxy-3,3'-bithiophenes. However, both synthetic pathways were less yielding than the one outlined in Scheme 1.

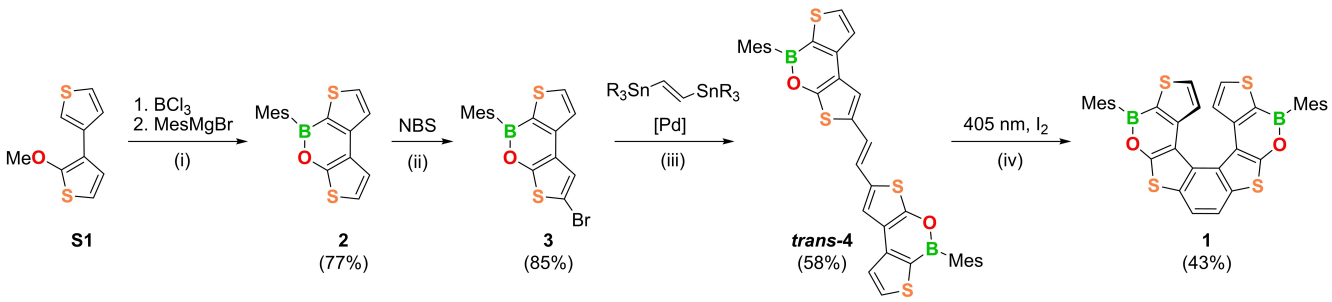

Scheme 1. Synthesis of the $(BO)_2$-doped tetrathia[7]helicene **1**. Reagents and conditions. i) 1. 1.5 equiv BCl_3, 1.2 equiv [nBu$_4$N]I, 1.0 equiv Et$_3$N, chlorobenzene, 135 °C, 24 h; 2. 3.0 equiv MesMgBr, THF, r.t., 1 h. (ii) 1.2 equiv *N*-bromosuccinimide (NBS), CH_2Cl_2, r.t., 12 h. (iii) 0.5 equiv R$_3$Sn(H)C=C(H)SnR$_3$ (R = *n*Bu), 12 mol% Pd(PPh$_3$)$_4$, toluene, 110 °C, 24 h. (iv) LED irradiation (405 nm), 1 equiv I_2, 100 equiv propylene oxide, C_6H_6, r.t., 2.5 h. Mes = 2,4,6-trimethylphenyl (mesityl).

Prior to subjecting *trans*-**4** to the Mallory photocyclization,[21] which requires *cis*-**4** as immediate precursor, the photochemical *trans*/*cis* isomerization of *trans*-**4** under irradiation with various light sources was quantitatively monitored by in situ ^{1}H NMR spectroscopy (Figures S1 and S2). A 405 nm LED performed the task most efficiently (*trans*/*cis* = 1:4 after 30 min; C_6D_6, r.t.) and was therefore used for the subsequent synthesis of the helicene **1**. After irradiating *trans*-**4** in the presence of I_2 and propylene oxide for 2.5 h (C_6H_6, r.t.), **1** was identified as sole product by thin-layer chromatography (TLC). Chromatographic purification finally gave **1** in 43 % yield. The role of propylene oxide is to quench the HI released during dehydrogenation of the photogenerated primary intermediate to form the aromatic ring. If the epoxide is omitted under otherwise identical conditions, an approximate 1:1 mixture of **1** and hydrogenated **4** with a saturated ethylene bridge (**4H$_2$**) is obtained (see paragraph 2.9.1 of the Supporting Information).[22]

In **1**, the former 1,2-ethenediyl CH groups resonate at $\delta(^1H) = 7.81$ and $\delta(^{13}C) = 119.0$. Moreover, the signal for the H atoms in vicinal positions to the 1,2-ethenediyl linker has disappeared and the resonance of the appended (now quaternary) C atoms is detectable at 117.3 ppm. The molecular structure of **1** was also characterized by single-crystal X-ray analysis (Figure 2). Two details of the synthetic approach to **1** are worth mentioning: (i) although the Mallory reaction is widely used in general helicene synthesis,[1] it has very rarely been successfully applied to the photocyclization of organoboranes,[23] likely because the reactive species I_2, HI, and propylene oxide are incompatible with most boron compounds. (ii) In most synthesis protocols for B-doped helicenes (such as **A**–**D**; Figure 1), the B atoms are introduced only in the final ring-closing step. The B–Het bonds must therefore be formed against the build-up of the steric strain that is ultimately responsible for the helical distortion. In our approach, the introduction of the BO moieties does not occur at this critical stage.

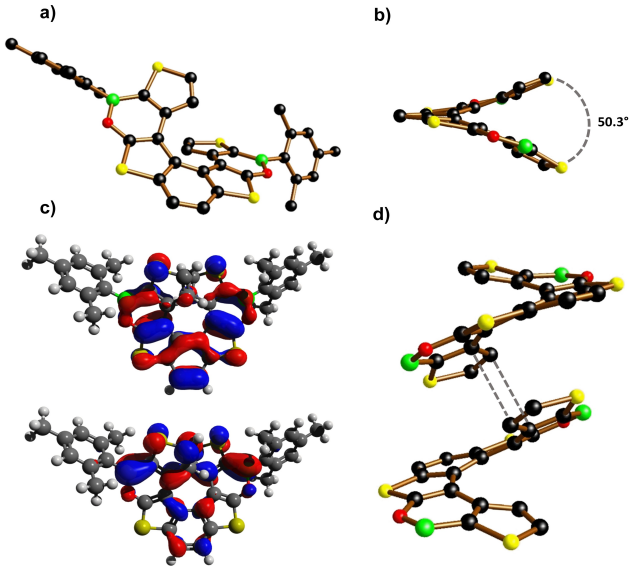

Figure 2. a) Front view of (*M*)-**1** with H atoms omitted for clarity.[24] b) Dihedral angle between the terminal SC_4 rings of (*M*)-**1**; H atoms and Mes rings are omitted for clarity. c) HOMO (top) and LUMO (bottom) of **1**, calculated at the B3LYP/6-31G* level. d) π-Stacking interaction between a (*P*)/(*M*)-pair of **1** with H atoms and Mes rings omitted for clarity. Grey lines indicate the shortest intermolecular C···C contacts; B: green, C: black, O: red, S: yellow spheres.

1 crystallizes as racemic mixture of the (*P*)- and (*M*)-enantiomers in the low-symmetric triclinic crystal system (Figure 2d). A dihedral angle of 50.26(9)° between the two terminal SC_4 rings is associated with intramolecular centroid···centroid distances of 4.153(6) Å (Figure 2b). The central C_6 ring is significantly twisted, as indicated by a torsion angle of 9.7° between the (H)C–C(H) vector and the opposite C–C bond. Unlike most Mes-protected B-doped polycyclic aromatic hydrocarbons (PAHs),[25] the Mes substituents in **1** are not orthogonally positioned to the attached B-containing heterocycles. The reason apparently lies in the neighboring O/S atoms and the annulated five-membered SC_4 ring, which impose a lower steric strain compared to CH fragments and annulated six-membered aryl units. Despite the smaller dihedral angles Mes//O–B–C = 59.0(5)°, 58.6(6)°, the contributions of the Mes substituents to the HOMO/LUMO frontier orbitals of **1** is negligible (Figure 2c). The B–O bond lengths of 1.402(4) and 1.401(5) Å are slightly larger than that in the reference compound 9-mesityl-10,9-oxaboraphenanthrene (av. B–O = 1.378 Å; av. Mes//O–B–C = 104.1(3) and 84.8(3)° for two crystallographically independent molecules in the asymmetric unit[26]). In the crystal, alternating molecules of (*P*)- and (*M*)-**1** form infinite rods by means of π-stacking interactions between SC_4 rings with shortest intermolecular C···C contacts of 3.427(5) and 3.457(4) Å (grey lines in Figure 2d; in this respect, the packing of (*P*)-/(*M*)-**1** and **E** are the same). Remarkably, the shortest intermolecular S···S distances are smaller than the intramolecular ones (3.9911(14) and 5.8156(2) Å, respectively).

Cyclic voltammograms were recorded in THF with [*n*Bu$_4$N][PF$_6$] as supporting electrolyte and are referenced against the ferrocene/ferricinium couple (FcH/FcH$^+$). In the cathodic scan, **1** shows two irreversible redox events with peak potentials of $E_{pc} = -2.83$ and -3.01 V (Table 1).

For comparison, the substructure **2** is somewhat harder to reduce with an E_{pc} value of -2.96 V. When two redox-active **2**-type sites are connected via a 1,2-ethenediyl bridge (*cf.* *trans*-**4**), the first reduction event at $E_{1/2} = -2.54$ V becomes quasi-reversible while the second remains largely irreversible ($E_{pc} = -2.90$ V). We attribute the easier reduction of *trans*-**4** relative to **2** to the more extended π-conjugation pathway in the former (*trans*-**4** adopts a fully planar structure in the solid state[27]). This interpretation is supported by the fact that the redox potential of saturated **4H$_2$** (1,2-ethanediyl bridge) is again cathodically shifted to $E_{pc} = -2.90$ V. In summary, the degree of electronic communication between the two **2**-type sites in the helically twisted compound **1** appears to be lower than in its planar precursor *trans*-**4**.

In *c*-hexane, **1** exhibits a structured UV/Vis absorption band with the most bathochromic shoulder appearing at

Table 1: Photophysical and electrochemical data of the compounds **1**, *trans*-**4**, **4H$_2$**, and **2**. Optical measurements were performed in *c*-hexane, and electrochemical measurements were performed in THF (r.t., supporting electrolyte: [*n*Bu$_4$N][PF$_6$] (0.1 M), scan rate 200 mV s^{-1}).

	λ_{max} [nm]	λ_{em}[a] [nm]	Φ_{PL}[b] [%]	E_{pc} [V]	E_g^{opt}[c] [eV]	E_{LUMO}[d] [eV]
1	269 330 341 359 374[e] (*363*)[f]	392 411	6 4[g]	−2.83 −3.01	3.16	–
trans-**4**	278 344[e] 364 383 403 (*395*)[f]	419 443	11 13[g]	−2.54[h] −2.90	2.93	−2.26
4H$_2$	318[e] 326 342[e]	374 388	7 7[g]	−2.90	3.51	—
2	313[e] 320 335[e] (*301*)[f]	366 380	6 9[g]	−2.96	3.57	—

[a] Resolved vibrational fine structure. [b] Quantum yields were determined by using a calibrated integrating sphere. [c] Optical band gap $E_g^{opt} = 1240/\lambda_{onset}$. [d] $E_{LUMO} = -4.8\ eV - E_{1/2}^{Red1}$ (FcH/FcH$^+$ = −4.8 eV vs vacuum level). [e] Shoulder. [f] Computed value (TD-DFT). [g] Quantum yields measured in THF. [h] $E_{1/2}$ value of the quasi-reversible process.

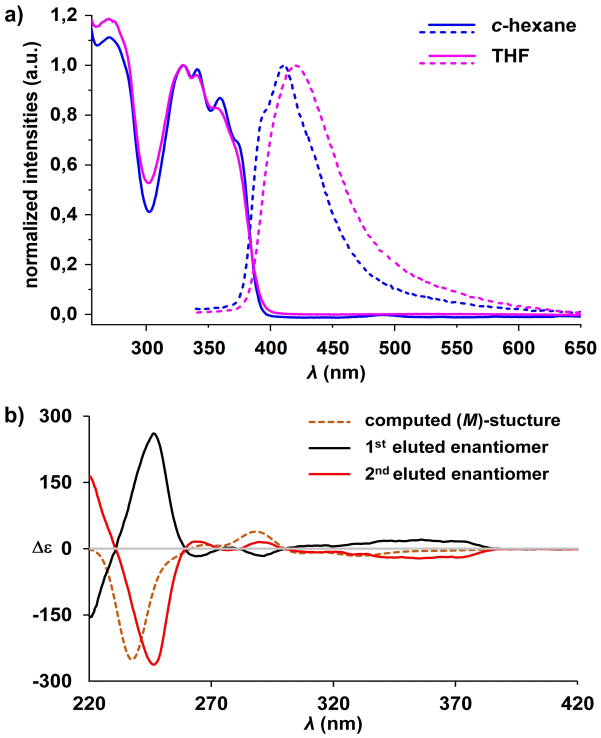

Figure 3. a) Normalized absorption and emission spectra of **1** in *c*-hexane (blue traces) and THF (pink traces). b) Circular dichroism (CD) spectra of the first (black trace) and the second (red trace) eluted enantiomer of **1**, recorded in *n*-hexane/CH_2Cl_2 (95:5) at 20 °C. Computed CD spectrum for the optimized (*M*)-structure (orange dashed trace; multiplied by a factor of 1.5).

374 nm (Figure 3a, blue trace; Table 1). For comparison, the corresponding shoulder in the spectrum of tetrathia-[7]helicene **E** is found at 392 nm.[28] **1** is a blue emitter and its emission band shows a partly resolved vibrational fine structure with the most hypsochromic shoulder at 411 nm; the photoluminescence quantum efficiency is $\Phi_{PL} = 6\,\%$ (*c*-hexane; *cf.* tetrathia[7]helicene: $\lambda_{em} \approx 405$ nm, $\Phi_{PL} = 5\,\%$).[29] We therefore conclude that BO-doping does not have a major influence on the electronic spectra of **E**. The reference systems **2**, **4H$_2$**, and *trans*-**4** absorb/emit at 335/366 nm, 342/374 nm, and 403/419 nm, respectively (Table 1). According to time-dependent density functional theory (TD-DFT) calculations, the first transitions of **1**, *trans*-**4**, and **2** are HOMO→LUMO transitions (Table 1, see also Tables S10–S12, Figure S55, and paragraph 7.1 of the Supporting Information). Taken together, these results confirm that **1** has a much more delocalized π-electron system than **2** and **4H$_2$**, but the effective conjugation length is smaller than for *trans*-**4**.

The (*P*)-/(*M*)-enantiomers of **1** were resolved by chiral stationary phase high-performance liquid chromatography (CSP-HPLC) on a Chiralpak IA column, using *n*-hexane/CH_2Cl_2 (95:5) as eluent (Figure 4a, blue trace).[27]

Preliminary racemization tests showed that the enantiomers of **1** are stereochemically stable at room temperature. Hence, the analytical HPLC resolution was scaled up to the semipreparative level using the same eluent. By definition, two enantiomers of the same compound have the same chemical and physical properties. In the following we will focus on the second eluted enantiomer, which we isolated in slightly higher enantiomeric excess (*e.e.* = 97.4 %, $R_t \approx 8$ min; Figure 4a, red trace). The collected fractions containing only the second eluted enantiomer were combined and evaporated at room temperature. The solid residue was dissolved in decalin and subjected to thermal racemization at 80 °C. The changes in the enantiomeric excess of the sample were monitored by CSP-HPLC (Figure 4b). The racemization process was monitored by the decrease in the enantiomeric excess of the sample. The interconversion of the two enantiomers proceeded smoothly: after only 13 min, the *e.e.* of the sample had dropped from 97.4 % to 80.6 % and the elution peak of the first enantiomer ($R_t \approx 6$ min) began to emerge (Figure 4b, purple trace). The *e.e.* data were collected over 64 min and used to determine the enantiomerization constant $k_{enant} = 8.15 \times 10^{-5}\ s^{-1}$ and the associated free energy of activation $\Delta G_{enant}^{\ddagger} = 27.4 \pm 0.1$ kcal mol^{-1} (at 353 K).[27,30]

The $\Delta G_{enant}^{\ddagger}$ value of the (BO)$_2$-doped tetrathia-[7]helicene **1** is considerably lower than the corresponding values determined for the enantiomerization of the parent tetrathia[7]helicene **E** ($\Delta G_{enant}^{\ddagger} = 39.4$ kcal mol^{-1})[31] and even carbo[6]helicene ($\Delta G_{enant}^{\ddagger} = 36.4$ kcal mol^{-1}).[32] Thus, the formal replacement of two C=C bonds by B=O bonds within the helical framework apparently increases the

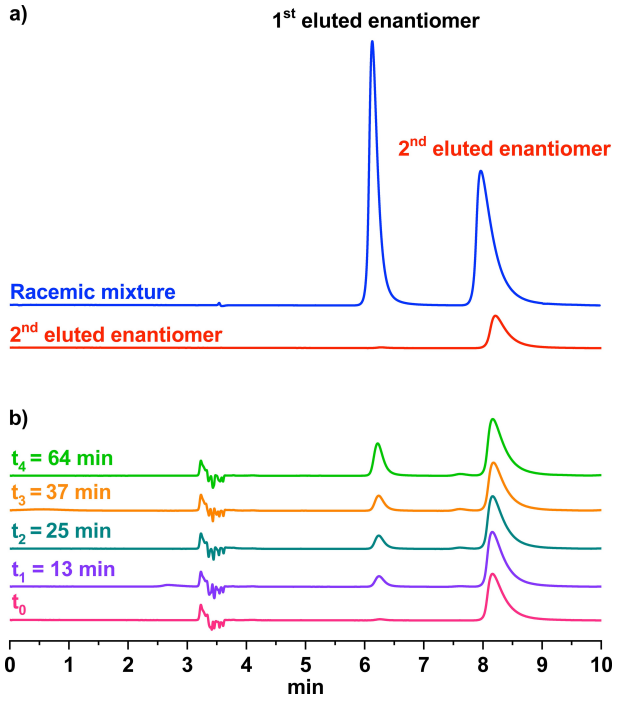

Figure 4. a) Analytical HPLC resolution of **1** (stationary phase: Chiralpak IA, mobile phase: *n*-hexane/CH_2Cl_2 (95:5), flow rate = 1.0 mL min^{-1}, 25 °C). b) Thermal racemization studies conducted on the second eluted enantiomer in decalin at 80 °C; solvent peak: $R_t \approx 3$ min.

flexibility of the molecular scaffold, consistent with the lower double-bond character of the latter.

Circular dichroism spectra recorded in *n*-hexane/CH_2Cl_2 (95:5) at 20 °C show a perfect mirror-image relationship between the first and second eluted enantiomer of **1** (Figure 3b, black and red trace); the optical rotation values are +97.7° and −97.5°, respectively.

To determine the absolute configurations of the two eluted enantiomers, the (*M*)-structure of **1** was optimized at the M06/6-311g G(d,p) level of theory. Only one energy minimum was obtained, and no other stable conformer was found, even with regard to possible different orientations of the Mes groups. The optimized gas-phase structure (C_2 symmetry) compares well with the crystallographically determined molecular geometry; the experimentally observed marked deviation of the dihedral angle Mes//O–B–C from 90° is qualitatively reproduced (calcd. 65.5°; av. exptl. 58.8°). The CD spectrum of (*M*)-**1** was calculated by TD-DFT at the same level of theory (Figure 3b, orange dashed trace). The agreement between the computed and one of the experimental CD spectra allows us to assign the (*M*)-configuration with certainty to the second eluted enantiomer ($R_t \approx 8$ min): good correspondence is observed for the broad negative feature centered at 350 nm, which can be attributed to the first three transitions with weak negative rotational strength (Figures 3b and S54). The two weak positive peaks experimentally observed at 293 and 265 nm are also well reproduced, as is the intense negative feature at 247 nm (calcd. 240 nm). The relatively small rotational strength computed for the first transition (HOMO→LUMO) is due to the fact that the electric and magnetic transition dipole moments are nearly perpendicular to each other. The CD spectrum of (*M*)-**1** is different from those of typical helicenes[33] and thiahelicenes,[34] in that it shows only weak features in the 370–260 nm range (Figure S53), but with a more intense absorption feature for the first electronic transition (Figures S54, S55, and Tables S10, S11). This is another example for the well-known fact that the lowest-energy transitions of helicenes are substituent-sensitive,[33] while the overall shape of the spectrum is determined by the helicene backbone.

The energy barrier for enantiomerization of **1** was computed by optimizing the ground state of (*M*)-**1** and the transition state to (*P*)-**1** at the PBE1-PBE/TZVP level with empirical dispersion corrections.[35] The obtained enantiomerization barrier of 35 kcal mol^{-1} is about 8 kcal mol^{-1} higher than the experimentally found value of $\Delta G_{enant}^{\ddagger} = 27.4 \pm 0.1$ kcal mol^{-1} (at 353 K);[36] the same barrier was obtained for the model compound **1*** carrying H atoms in place of the Mes groups. We also compared the enantiomerization barrier of the model compound **1*** with those of carbo-[6]helicene and tetrathia[7]helicene **E** by performing a relaxed interconversion scan considering also diffuse functions at the PBE1-PBE/6-311++G(d,p) level with empirical dispersion corrections (Figures S56 and S57). Despite the seven-ring backbone of **1***, its barrier is the lowest of the three compounds (**1***: 35 kcal mol^{-1}, carbo[6]helicene: 38 kcal mol^{-1}, and **E**: 40 kcal mol^{-1}). A comparison of the minimum and transition-state structures of **1*** and **E** indicates that the smaller double-bond character of the B=O pairs indeed allows for greater flexibility of the six-membered heterocycle compared to a carbonaceous benzene ring (Figure S58).

Conclusion

The $(BO)_2$-doped tetrathia[7]helicene **1** was obtained via an efficient four-step synthesis, including a Mallory photocyclization step, which has rarely been used for the synthesis of B-containing polycyclic aromatic hydrocarbons. Despite its configurational stability at room temperature, the racemization and enantiomerization barriers of **1** are significantly lower than that of its non-doped congener, the tetrathia[7]helicene **E**. This is presumably due to the weaker π-donor bond within the BO pair, which renders the BOC_4 heterocycles more conformationally flexible than benzene rings. To date, boron-heteroatom doping has been performed mainly on planar polycyclic aromatic hydrocarbons, where conformational flexibility is not an issue, and is therefore considered primarily as a tool for manipulating the electronic structures of π-electron systems. Our results now indicate that the incorporation of BO pairs can also be a means of influencing the mechanical rigidity of polyaromatic entities. With regard to the optoelectronic properties of helicenes, the high application potential of circularly polarized luminescence is particularly well recognized. Even though **1** has a rather low photoluminescence quantum efficiency of $\Phi_{PL} = 6\,\%$, its synthesis protocol should allow

manifold optimizations in the future, such as BN doping, inversion of the BO/BN vectors, or facile late-stage derivatization at the terminal thiophene rings.

Acknowledgements

L. M. is grateful to the University of Milan for providing a Ph.D. scholarship and to the Goethe-Universität Frankfurt for enabling a binational joint Ph.D. programme. The authors thank Dr. Alexander Virovets for helpful discussions regarding X-ray crystallography. Open Access funding enabled and organized by Projekt DEAL.

Conflict of Interest

The authors declare no conflict of interest.

Data Availability Statement

The data that support the findings of this study are available from the corresponding authors upon request.

Keywords: Boron · Chirality · Doping · Helicenes · Thiophenes

[1] a) Y. Shen, C.-F. Chen, *Chem. Rev.* **2012**, *112*, 1463–1535; b) M. Gingras, *Chem. Soc. Rev.* **2013**, *42*, 1051–1095; c) J. R. Brandt, F. Salerno, M. J. Fuchter, *Nat. Chem. Rev.* **2017**, *1*, 0045; d) K. Dhbaibi, L. Favereau, J. Crassous, *Chem. Rev.* **2019**, *119*, 8846–8953; e) P. Ravat, *Chem. Eur. J.* **2021**, *27*, 3957–3967.

[2] a) A. Borissov, Y. K. Maurya, L. Moshniaha, W. S. Wong, M. Żyła-Karwowska, M. Stępień, *Chem. Rev.* **2022**, *122*, 565–788; b) M. Stępień, E. Gońka, M. Żyła, N. Sprutta, *Chem. Rev.* **2017**, *117*, 3479–3716; c) A. Narita, X.-Y. Wang, X. Feng, K. Müllen, *Chem. Soc. Rev.* **2015**, *44*, 6616–6643.

[3] a) K. Schickedanz, T. Trageser, M. Bolte, H. W. Lerner, M. Wagner, *Chem. Commun.* **2015**, *51*, 15808–15810; b) F. Miyamoto, S. Nakatsuka, K. Yamada, K. I. Nakayama, T. Hatakeyama, *Org. Lett.* **2015**, *17*, 6158–6161; c) J. Radtke, K. Schickedanz, M. Bamberg, L. Menduti, D. Schollmeyer, M. Bolte, H. W. Lerner, M. Wagner, *Chem. Sci.* **2019**, *10*, 9017–9027.

[4] a) T. Hatakeyama, S. Hashimoto, T. Oba, M. Nakamura, *J. Am. Chem. Soc.* **2012**, *134*, 19600–19603; b) Y. Si, G. Yang, *J. Mater. Chem. C* **2013**, *1*, 2354–2361.

[5] For related BN-helicenes, see: a) A. Abengózar, P. García-García, D. Sucunza, A. Pérez-Redondo, J. J. Vaquero, *Chem. Commun.* **2018**, *54*, 2467–2470; b) Z. Sun, C. Yi, Q. Liang, C. Bingi, W. Zhu, P. Qiang, D. Wu, F. Zhang, *Org. Lett.* **2020**, *22*, 209–213; c) K. Yuan, D. Volland, S. Kirschner, M. Uzelac, G. S. Nichol, A. Nowak-Król, M. J. Ingleson, *Chem. Sci.* **2022**, *13*, 1136–1145; d) M. Yang, I. S. Park, T. Yasuda, *J. Am. Chem. Soc.* **2020**, *142*, 19468–19472; e) J. K. Li, X. Y. Chen, Y. L. Guo, X. C. Wang, A. C. H. Sue, X. Y. Cao, X. Y. Wang, *J. Am. Chem. Soc.* **2021**, *143*, 17958–17963.

[6] a) T. Katayama, S. Nakatsuka, H. Hirai, N. Yasuda, J. Kumar, T. Kawai, T. Hatakeyama, *J. Am. Chem. Soc.* **2016**, *138*, 5210–5213; b) X. Y. Wang, A. Narita, W. Zhang, X. Feng, K. Müllen, *J. Am. Chem. Soc.* **2016**, *138*, 9021–9024; c) X. Y. Wang, T. Dienel, M. Di Giovannantonio, G. B. Barin, N. Kharche, O. Deniz, J. I. Urgel, R. Widmer, S. Stolz, L. H. De Lima, M. Muntwiler, M. Tommasini, V. Meunier, P. Ruffieux, X. Feng, R. Fasel, K. Müllen, A. Narita, *J. Am. Chem. Soc.* **2017**, *139*, 4671–4674; d) Z. Zhou, X. Y. Wang, Z. Wei, K. Müllen, M. A. Petrukhina, *Angew. Chem. Int. Ed.* **2019**, *58*, 14969–14973; *Angew. Chem.* **2019**, *131*, 15111–15115.

[7] For B,O-helicenes without direct B–O bond, see: H. Hirai, K. Nakajima, S. Nakatsuka, K. Shiren, J. Ni, S. Nomura, T. Ikuta, T. Hatakeyama, *Angew. Chem. Int. Ed.* **2015**, *54*, 13581–13585; *Angew. Chem.* **2015**, *127*, 13785–13789.

[8] J. Full, S. P. Panchal, J. Götz, A. M. Krause, A. Nowak-Król, *Angew. Chem. Int. Ed.* **2021**, *60*, 4350–4357; *Angew. Chem.* **2021**, *133*, 4396–4403.

[9] For related heterohelicenes, see: a) C. Shen, M. Srebro-Hooper, M. Jean, N. Vanthuyne, L. Toupet, J. A. G. Williams, A. R. Torres, A. J. Riives, G. Muller, J. Autschbach, J. Crassous, *Chem. Eur. J.* **2017**, *23*, 407–418; b) Z. Domínguez, R. López-Rodríguez, E. Álvarez, S. Abbate, G. Longhi, U. Pischel, A. Ros, *Chem. Eur. J.* **2018**, *24*, 12660–12668; c) F. Full, Q. Wölflick, K. Radacki, H. Braunschweig, A. Nowak-Król, *Chem. Eur. J.* **2022**, *28*, e202202280; d) F. Full, M. J. Wildervanck, D. Volland, A. Nowak-Król, *Synlett* **2022**, *33*, https://doi.org/10.1055/a-1914-1799.

[10] R. B. Alnoman, S. Rihn, D. C. O'Connor, F. A. Black, B. Costello, P. G. Waddell, W. Clegg, R. D. Peacock, W. Herrebout, J. G. Knight, M. J. Hall, *Chem. Eur. J.* **2016**, *22*, 93–96.

[11] For related heterohelicenes, see: a) H. Kim, A. Burghart, M. B. Welch, J. Reibenspies, K. Burgess, *Chem. Commun.* **1999**, 1889–1890; b) A. Loudet, R. Bandichhor, K. Burgess, A. Palma, S. O. McDonnell, M. J. Hall, D. F. O'Shea, *Org. Lett.* **2008**, *10*, 4771–4774; c) M. Saikawa, T. Nakamura, J. Uchida, M. Yamamura, T. Nabeshima, *Chem. Commun.* **2016**, *52*, 10727–10730.

[12] a) S. Maiorana, A. Papagni, E. Licandro, R. Annunziata, P. Paravidino, D. Perdicchia, C. Giannini, M. Bencini, K. Clays, A. Persoons, *Tetrahedron* **2003**, *59*, 6481–6488; b) H. Nakagawa, A. Obata, K.-I. Yamada, H. Kawazura, *J. Chem. Soc. Perkin Trans. 2* **1985**, 1899–1903; c) E. Licandro, S. Cauteruccio, D. Dova, *Adv. Heterocycl. Chem.* **2016**, *118*, 1–46.

[13] General information on thiaheterohelicenes is reviewed in: a) S. K. Collins, M. P. Vachon, *Org. Biomol. Chem.* **2006**, *4*, 2518–2524; b) Y. H. Tian, G. Park, M. Kertesz, *Chem. Mater.* **2008**, *20*, 3266–3277. Rare examples of CPL-active thiahelicenes are mentioned here: c) B. C. Baciu, P. J. Bronk, T. de Ara, R. Rodriguez, P. Morgante, N. Vanthuyne, C. Sabater, C. Untiedt, J. Autschbach, J. Crassous, A. Guijarro, *J. Mater. Chem. C* **2022**, *10*, 14306–14318.

[14] B. Champagne, J. M. André, E. Botek, E. Licandro, S. Maiorana, A. Bossi, K. Clays, A. Persoons, *ChemPhysChem* **2004**, *5*, 1438–1442.

[15] H. Yu, B. Xu, T. M. Swager, *J. Am. Chem. Soc.* **2003**, *125*, 1142–1143.

[16] M. Gross, D. C. Müller, H. G. Nothofer, U. Scherf, D. Neher, C. Bräuchle, K. Meerholz, *Nature* **2000**, *405*, 661–665.

[17] T. M. Pappenfus, R. J. Chesterfield, C. D. Frisbie, K. R. Mann, J. Casado, J. D. Raff, L. L. Miller, *J. Am. Chem. Soc.* **2002**, *124*, 4184–4185.

[18] L. Menduti, C. Baldoli, S. Arnaboldi, A. Dreuw, D. Tahaoglu, A. Bossi, E. Licandro, *ChemistryOpen* **2022**, *11*, e202100265.

[19] K. Shigemori, M. Watanabe, J. Kong, K. Mitsudo, A. Wakamiya, H. Mandai, S. Suga, *Org. Lett.* **2019**, *21*, 2171–2175.

[20] [nBu$_4$N]I was added to promote the demethylation of the intermediate ArO(Me)-borane adduct by the strongly nucleophilic I^- ion: S. A. Iqbal, J. Pahl, K. Yuan, M. J. Ingleson, *Chem. Soc. Rev.* **2020**, *49*, 4564–4591.

[21] K. B. Jørgensen, *Molecules* **2010**, *15*, 4334–4358.

[22] Formal H_2 transfer during photocyclization reactions using I_2, but no HI scavenger (such as propylene oxide), has been reported for stilbene derivatives: L. Liu, B. Yang, T. J. Katz, M. K. Poindexter, *J. Org. Chem.* **1991**, *56*, 3769–3775.

[23] a) V. M. Hertz, J. G. Massoth, M. Bolte, H. W. Lerner, M. Wagner, *Chem. Eur. J.* **2016**, *22*, 13181–13188; b) W. Sun, J. Guo, Z. Fan, L. Yuan, K. Ye, C. Dou, Y. Wang, *Angew. Chem. Int. Ed.* **2022**, *61*, e202209271; *Angew. Chem.* **2022**, *134*, e202209271. For the synthesis of helicenyl boronates by photocyclization, see: c) N. Hellou, A. Macé, C. Martin, V. Dorcet, T. Roisnel, M. Jean, N. Vanthuyne, F. Berrée, B. Carboni, J. Crassous, *J. Org. Chem.* **2018**, *83*, 484–490; d) A. Macé, N. Hellou, J. Hammoud, C. Martin, E. S. Gauthier, L. Favereau, T. Roisnel, E. Caytan, G. Nasser, N. Vanthuyne, J. A. Gareth Williams, F. Berrée, B. Carboni, J. Crassous, *Helv. Chim. Acta* **2019**, *102*, e1900044; e) A. Macé, K. Hamrouni, E. S. Gauthier, M. Jean, N. Vanthuyne, L. Frédéric, G. Pieters, E. Caytan, T. Roisnel, F. Aloui, M. Srebro-Hooper, B. Carboni, F. Berrée, J. Crassous, *Chem. Eur. J.* **2021**, *27*, 7959–7967.

[24] Deposition numbers 2211410 (for **1**), CCDC 2211405 (for **2**), CCDC 2211406 (for **3**), CCDC 2211409 (for *trans*-**4**), CCDC 2211407 (for **5**), CCDC 2211408 (for **6**) and CCDC 2211411 (for $\mathbf{4H_2}$) contain the supplementary crystallographic data for this paper. These data are provided free of charge by the joint Cambridge Crystallographic Data Centre and Fachinformationszentrum Karlsruhe Access Structures service.

[25] For representative examples, see: C. Hoffend, M. Diefenbach, E. Januszewski, M. Bolte, H. W. Lerner, M. C. Holthausen, M. Wagner, *Dalton Trans.* **2013**, *42*, 13826–13837.

[26] A. Budanow, E. v. Grotthuss, M. Bolte, M. Wagner, H. Lerner, *Tetrahedron* **2016**, *72*, 1477–1484.

[27] Full details are provided in the Supporting Information.

[28] M. B. Groen, H. Wynberg, *J. Am. Chem. Soc.* **1971**, *93*, 2968–2974.

[29] T. Caronna, M. Catellani, S. Luzzati, L. Malpezzi, S. V. Meille, A. Mele, C. Richter, R. Sinisi, *Chem. Mater.* **2001**, *13*, 3906–3914.

[30] a) L. Meca, D. Reha, Z. Havlas, *J. Org. Chem.* **2003**, *68*, 5677–5680; b) D. C. Patel, R. M. Woods, Z. S. Breitbach, A. Berthod, D. W. Armstrong, *Tetrahedron: Asymmetry* **2017**, *28*, 1557–1561.

[31] K. Yamada, H. Nakagawa, H. Kawazura, *Bull. Chem. Soc. Jpn.* **1986**, *59*, 2429–2432.

[32] R. H. Janke, G. Haufe, E. U. Würthwein, J. H. Borkent, *J. Am. Chem. Soc.* **1996**, *118*, 6031–6035.

[33] a) Y. Nakai, T. Mori, K. Sato, Y. Inoue, *J. Phys. Chem. A* **2012**, *116*, 7372–7385; b) S. Abbate, G. Longhi, F. Lebon, E. Castiglioni, S. Superchi, L. Pisani, F. Fontana, F. Torricelli, T. Caronna, C. Villani, R. Sabia, M. Tommasini, A. Lucotti, D. Mendola, A. Mele, D. A. Lightner, *J. Phys. Chem. C* **2014**, *118*, 1682–1695.

[34] a) V. Pelliccioli, F. Cardano, G. Renno, F. Vasile, C. Graiff, G. Mazzeo, A. Fin, G. Longhi, S. Abbate, A. Rosetti, G. Viscardi, E. Licandro, S. Cauteruccio, *Catalysts* **2022**, *12*, 366; b) S. Abbate, G. Longhi, T. Mori, in *Helicenes Synth. Prop. Appl.* (Eds.: J. Crassous, I. Stará, I. Starý), Wiley-VCH, Weinheim, **2022**, pp. 373–394.

[35] a) J. Barroso, J. L. Cabellos, S. Pan, F. Murillo, X. Zarate, M. A. Fernandez-Herrera, G. Merino, *Chem. Commun.* **2018**, *54*, 188–191; b) S. Grimme, J. Antony, S. Ehrlich, H. Krieg, *J. Chem. Phys.* **2010**, *132*, 154104.

[36] Enantiomerization is the reversible conversion of a single enantiomer into the other one. The corresponding rate constant is k_{enant}. Racemization is the irreversible conversion of a sample of single enantiomers or of a non-racemic mixture of enantiomers into the racemate. The corresponding rate constant is k_{rac}. Comparison of calculated and experimental energy barriers was done using the enantiomerization barrier obtained from k_{enant}, which is calculated from the experimentally determined k_{rac} according to: $k_{enant} = 0.5k_{rac} = 8.15 \times 10^{-5}\,s^{-1}$. The free energy for the enantiomerization process ($\Delta G_{enant}^{\ddagger}$) was obtained by using the Eyring equation and setting a transmission coefficient equal to 1.

Manuscript received: October 20, 2022
Accepted manuscript online: November 21, 2022
Version of record online: December 20, 2022